Analysis of Self-het OFDM Enhancements for 60GHz Indoor RF Channels

Nirmal Fernando
ECSE Monash Univ., Australia
nirmal.fernando@monash.edu

Yi Hong
ECSE Monash Univ., Australia
yi.hong@monash.edu

Emanuele Viterbo
ECSE Monash Univ., Australia
emanuele.viterbo@monash.edu

***Abstract*—In this paper, we consider two enhancements for self-heterodyne OFDM (Self-Het OFDM): *subcarrier pairing* and *smart carrier positioning* (SCP). We analyze their performance over a practical 60 GHz indoor RF channel. This channel deviates from the standard AWGN and Rayleigh fading models for Line of Sight (LoS) and Non LoS. We show that for NLoS channels they can jointly improve the diversity order and performance by 7.7 dB at BER of 10^{-2}, when compared to the standard self-het OFDM. Similar improvements are observed for channels with strong LoS components.**

Keywords: Precoding, diversity, OFDM, self-heterodyne, multipath fading, non-coherent detection.

I. Introduction

In millimeter-wave and terahertz communications, the implementation of stable and low complexity receivers is technically challenging due to instabilities of oscillators and mixers. Hence, significant levels of phase noise are commonly experienced in RF receivers even if advanced frequency stabilization techniques [2], [3] are used.

Conventional orthogonal frequency division multiplexing (OFDM) is a popular technique to combat multipath fading for wireless communications. However, for the millimeter-wave and terahertz communications, OFDM is known to have performance degradation due to high levels of residual phase noise at such high frequencies [1]. In 2001, Shoji *et. al.* proposed self-heterodyne OFDM (self-het OFDM) in [6], [7] as an alternative OFDM technique to compensate these high-level oscillator instabilities in 60 GHz RF bands. In self-het OFDM, the transmitter sends both the local RF carrier and the OFDM subcarriers, and a square-law circuitry (self-mixing) is used at the receiver to down-convert the RF signal. This removes the needs of a local carrier, carrier frequency correction and carrier phase recovery. Since the transmitted local RF carrier phase is synchronous with the OFDM subcarriers, self-het OFDM receivers have theoretically zero phase noise and is extremely stable. However, this advantage comes at the cost of a 50% reduction in rate.

For self-het OFDM, we previously proposed the following two enhancements:

Smart carrier positioning (SCP): It was shown in [11] that the entire OFDM symbol subjects to an outage, if the local RF carrier experiences deep fading. In the SCP, the receiver estimates the optimum RF carrier location (i.e. carrier frequency) using the available channel state information (CSI), and sends it back to the transmitter. Hence, the SCP can significantly reduce the occurrence of this outage.

Subcarrier pairing scheme [12]: In self-het OFDM, unbalance signal-to-interference noise ratios (SINRs) occur over all subcarriers. The subcarrier pairing is performed across those OFDM subcarriers by grouping *good* OFDM subcarriers with high SINRs and *bad* OFDM subcarriers with low SINRs, in order to improve the overall system performance [12].

In our previous work, we analyzed these enhancements for self-het OFDM over Rayleigh fading channels. However, in millimeter and terahertz channels, the channel fading characteristics may deviate from Rayleigh fading, and more accurate channel models are required for such system performance evaluations. One such model was proposed in [9] by modifying the conventional Saleh-Valenzuela (SV) model [10] and experimentally estimating the relevant parameters for 60 GHz indoor RF channels. In this paper, we adopt this channel model and we analyze the performance of the enhanced self-het OFDM using SCP and subcarrier pairing over such channels.

The paper is organized as follows. In Section II, we review the 60 GHz indoor RF channel model and self-het OFDM systems. In Section III, we present the two enhancements: SCP and subcarrier pairing. In Section IV, we show the simulation results on these enhancements over 60 GHz indoor RF channels. Finally, we draw the conclusions in Section V.

II. System Model

A. Channel Model

A modified Saleh-Valenzuela (SV) model is presented in [9] for 60 GHz indoor (millimeter-wave) RF communication channels. This model is based on a combination of the conventional SV-model [10] and a modified two-path model [9]. This is because that the conventional SV-model does not capture the line of sight (LoS) components appearing in such channels, and the single reflection rays are as strong as LoS, as demonstrated in [9]. We let $h_{\text{two}}(t)$ and $h_{\text{sv}}(t)$ be the impulse response of two-path channel model and the impulse response of SV model, respectively. Then the combined channel impulse response is given by [9]

$$h_{\text{sv}'}(t) = h_{\text{two}}(t) + \sqrt{\frac{1}{K+1}} h_{\text{sv}}(t) \tag{1}$$

978-1-4673-4675-7/13/$31.00 ©2013 IEEE

where K is the Rician K-factor. It is shown in [9] that the impulse response of the two-path channel model

$$h_{\text{two}}(t) = \alpha\delta(t)$$

is considered to be a random variable, where α is assumed to follow a Gaussian distribution, $\alpha \sim \mathcal{N}(\sqrt{K/(K+1)}, \sigma_\alpha^2)$, and σ_α denotes the standard deviation of α. The impulse response of the SV-channel model is given by [10]

$$h_{\text{sv}}(t) = \sum_{l=1}^{L}\sum_{m=1}^{M_l} \xi_l \beta_{lm} e^{j\theta_{lm}} \delta(t - T_l - \tau_{lm}) \tag{2}$$

where L, M_l, T_l, τ_{lm} represent the total number of clusters of rays, the total number of rays in the l-th cluster, the arrival interval of the $l-$th cluster, the arrival interval of the m-th ray in the l-th cluster, respectively. The terms β_{lm} and θ_{lm} denote the amplitude and phase of the $m-$th ray at the $l-$th cluster. The term ξ_l denotes the amplitude of the $l-$th cluster of rays. Then the distributions of inter-cluster arrival times and inter-ray arrival times are given by [10]

$$\begin{aligned} P(T_l|T_{l-1}) &= \Lambda \exp\{-\Lambda(T_l - T_{l-1})\} \\ P(\tau_{lm}|\tau_{l(m-1)}) &= \lambda \exp\{-\lambda(\tau_{lm} - \tau_{l(m-1)})\} \end{aligned}$$

where Λ and λ denote the cluster and ray arrival rates, respectively, and $l, m > 0$. It was shown in [9] that the phase θ_{lm} follows a uniform distribution over $[0, 2\pi)$, and the average path gain is given by [9]

$$\Omega_{lm} = E[|\xi_l \beta_{lm}|^2] = \Omega_0 e^{-T_l/\Gamma} e^{-\tau_{lm}/\gamma} \tag{3}$$

where $\Omega_0 = |\xi_1\beta_{11}|^2$ and Γ, γ denote cluster and ray power-decay time constants, respectively. The amplitudes of ξ_l and β_{lm} in (2) follow two independent log-normal distributions with standard deviations σ_1 and σ_2, respectively. Hence, $|\xi_l\beta_{lm}|$ also follows a log-normal distribution, i.e., $(20\log_{10}(|\xi_l\beta_{lm}|) \sim \mathcal{N}(\mu_{lm}, \sigma_1^2 + \sigma_2^2))$, where

$$\mu_{lm} = \frac{10\ln(\Omega_0) - 10\left(\frac{T_l}{\Gamma} + \frac{\tau_{lm}}{\gamma}\right)}{\ln(10)} - \frac{\ln(10)(\sigma_1^2 + \sigma_2^2)}{20}.$$

The response of the k-th OFDM subcarrier can be obtained by taking the Fourier transform of (1), i.e.,

$$\begin{aligned} H_k &\triangleq H(f_c + k\Delta f) \\ &= \alpha + \sum_{l=1}^{L}\sum_{m=1}^{M_l} \xi_l\beta_{lm} e^{[-j\{2\pi(f_c + k\Delta f)(T_l + \tau_{lm}) - \theta_{lm}\}]} \end{aligned} \tag{4}$$

where Δf is the OFDM subcarrier spacing and f_c denotes the RF carrier frequency.

B. Self-het OFDM

A block diagram of the self-het OFDM communication system is shown in Fig. 1, where N, N_g and N_x denote the size of Inverse Fast Fourier Transform (IFFT), the number of subcarriers omitted, and the number of OFDM subcarriers used to encode information, respectively, and $N = N_g + N_x$.

At the transmitter, the information is first mapped to OFDM symbols X_k, $k = 1, ..., N_x$, using $M-$QAM signalling.

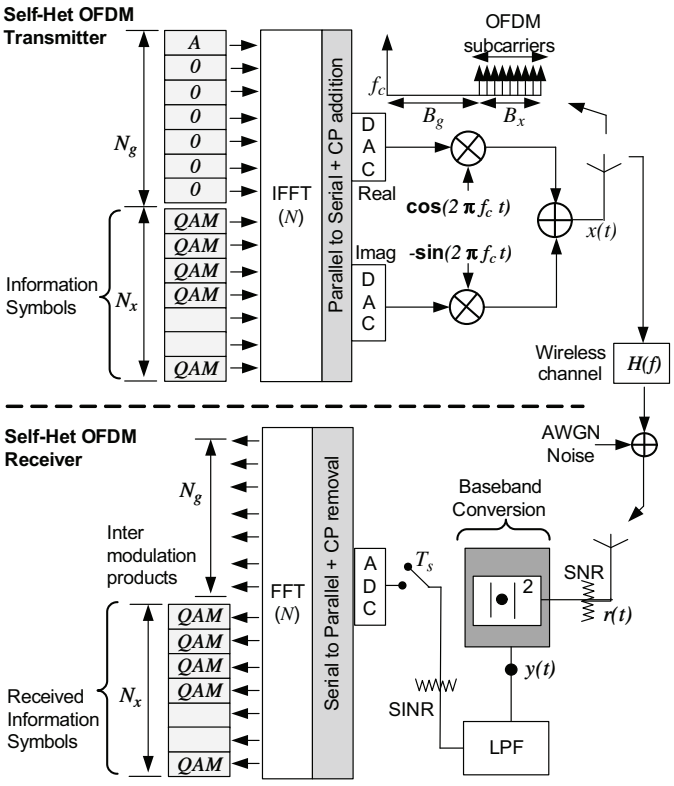

Fig. 1. Self-Het OFDM communication system

Those OFDM signals are then transmitted over N_x OFDM subcarriers, followed by the IFFT operation and the addition of the cyclic prefix (CP) with a length sufficient to avoid inter-symbol interference (ISI). Then both parallel-to-serial conversion and digital-to-analogue conversion are used to generate the continuous time-domain OFDM signal $s(t)$, i.e.,

$$s(t) = \Re\left\{\sum_{k=1}^{N_x} X_k e^{j2\pi(f_c + B_g + k\Delta f)t}\right\} \tag{5}$$

where $B_g = N_g\Delta f$ denotes the frequency gap between the carrier and the first OFDM subcarrier. The RF signal $x(t)$ is then generated as $x(t) = A\cos(2\pi f_c t) + s(t)$, where A is the RF carrier amplitude.

When the RF signal $x(t)$ is transmitted over the 60 GHz RF fading channel $h_{\text{sv}'}(t)$, given in (1), the received signal is given by

$$r(t) = h_{\text{sv}'}(t) * x(t) + n(t) \tag{6}$$

where $n(t) \sim \mathcal{N}(0, \sigma^2)$ is the additive white Gaussian noise (AWGN) with the noise power σ^2. At the receiver, the non-linear operation $y(t) = |r(t)|^2$ down-converts the passband signal to the baseband signal. Since the local RF carrier signal is embedded in the received signal, this down-conversion does not involve any local carrier generation, carrier frequency correction, and carrier phase recovery at the receiver. If the guard band B_g satisfies $B_g \geq B_x$, the information can be recovered completely by only considering the N_x OFDM

subcarriers, as shown in [11]. It was also shown in [11] that, since the non-linear down-conversion generates high frequency and DC components, a low pass filter (LPF) with a cutoff frequency $B_g + B_x$ and a DC filter are used before the sampling and the analog-to-digital conversion (ADC). Then, the CP removal, serial-to-parallel conversion and the FFT operation are performed to recover the information symbols carried over the N_x OFDM subcarriers, as illustrated in Fig. 1.

The equivalent discrete baseband model of self-het OFDM under multipath fading channels can be written as [11]

$$Y_k = AH_c{}^* H_k X_k + \hat{Z}_k \quad (7)$$

where Y_k, H_k, H_c, and $\hat{Z}_k$ are the received information symbol at the k-th OFDM subcarrier, the equivalent channel response at the k-th OFDM subcarrier, the equivalent channel response at the local RF carrier, and the equivalent noise component, respectively. In moderate and high SNR regions, the equivalent noise power of the k-th carrier can be given by [11]

$$\sigma^2_{\hat{Z}_k} = \sigma^2 A^2 \left(|H_c|^2 + \frac{\lambda(k)}{\eta N_x} \right) \quad (8)$$

where

$$\lambda(k) = \frac{2N_x}{N_x + N_g}(N_g + N_x - k)$$

and η denotes the local RF carrier-to-signal power ratio [11].

III. Enhancements of self-het OFDM

The channel model presented in Section II (A) is used to analyze the performance of the following two enhancements.

A. Smart Carrier Positioning Technique

In [11], we propose the *Smart Carrier Positioning* (SCP) technique to avoid transmitting the carrier in a deep fading scenario. As shown in (7), if the local RF carrier is transmitted over a bad channel (i.e. $|H_c| << 1$), the entire OFDM symbol experiences deep fading. Using the SCP, the local RF carrier can be selectively positioned either on the left or the right handside of the OFDM subcarriers, as shown in Fig. 2. We note that if the local RF carrier is placed in the right handside, the information subcarriers are transmitted in the lower band. In this case, the transmitted OFDM symbols must be $X_k{}^*$, instead of X_k, in order to receive the information symbols correctly, as shown in Fig. 2. In SCP, the carrier is placed in the $\hat{i}$-th position such that,

$$\hat{i} = \underset{\substack{i \in \{1,\ldots \frac{P}{2}, \\ N-\frac{P}{2},\ldots,N\}}}{\arg\max} \{|H_i|^2\} \quad (9)$$

where $|H_{\hat{i}}|^2$ is the channel gain at the carrier and P denotes the total number of potential carrier positions. Let $p = \hat{i}$, if the carrier is positioned on the left handside; and we let $p = N+1-\hat{i}$, if it is positioned on the right handside. Then we have $B_g = B_x = \Delta f(N+1-p)/2$, where $p \in \{1, 2, ..., P/2\}$. We note that the positioning strategy in (9) can be implemented at the transmitter with the known channel state information.

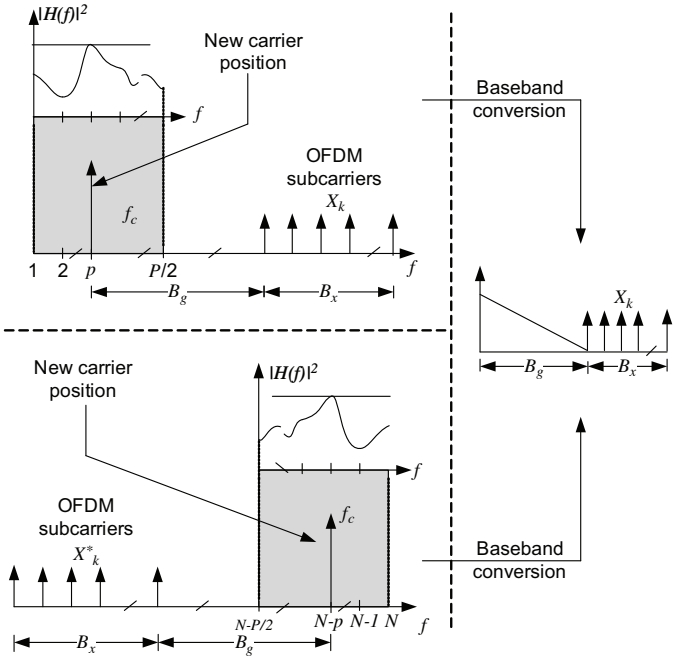

Fig. 2. Smart carrier positioning.

Otherwise, the position $\hat{i}$ is chosen at the receiver and can be fed back to the transmitter site. Furthermore, we note that the number of potential carrier positions required to achieve the optimum performance is very small [11]. Hence, the rate loss due to the allocation of the potential carrier position is almost negligible for OFDM systems with large number of subcarriers.

B. OFDM subcarrier pairing

In [12], we present a subcarrier pairing scheme to improve the overall bit error rate (BER) performance of self-het OFDM communications. As shown in (8), the equivalent noise power of the k-th carrier $\sigma^2_{\hat{Z}_k}$ depends on the subcarrier index k, where $\sigma^2_{\hat{Z}_k}$ decreases with k. Hence, unbalanced SINRs occurs in self-het OFDM subcarriers. Pairing, originally proposed in [13] for MIMO systems, can be used to pair good subcarriers with high SINRs and bad subcarriers with low SINRs, so that the overall system performance can be improved.

At the transmitter, information symbols are first grouped in pairs before the transmission using N_x OFDM subcarriers. Let $\Phi = \{(a_i, b_i), i = 1, ..., N_x/2\}$ be the set of *M*-QAM information symbol pairs transmitted over an OFDM symbol. To generate two pre-coded symbols, each symbol pair (a_i, b_i) is first multiplied by an $\exp(j\theta_i)$ where θ_i is the rotation angle for the i-th pair. Subsequently, IQ component interleaving [14] is performed across two precoded symbols (a_i, b_i) as

$$\begin{aligned} \hat{X}_{p_i} &= \Re\{a_i \exp(j\theta_i)\} + j\Re\{b_i \exp(j\theta_i)\} \\ \hat{X}_{q_i} &= \Im\{a_i \exp(j\theta_i)\} + j\Im\{b_i \exp(j\theta_i)\} \end{aligned} \quad (10)$$

to generate the coded symbol pairs $\Psi = \{(\hat{X}_{p_i}, \hat{X}_{q_i}), i = 1, ..., N_x/2\}$, where $\{(p_i, q_i), i = 1, ..., N_x/2\}$ denotes the

indices of each subcarrier pair, and it forms a partition of the N_x subcarriers. For example, one of the pairing methods can be

$$(p_i, q_i) = (i, N_x - i + 1) \quad i = 1, \ldots, N_x/2 \tag{11}$$

and we assume the pairing method in (11) for the remainder of the paper. As shown in [13], the overall BER performance can be improved by optimizing θ_i for each precoded symbol pair. Let γ_{p_i} and γ_{q_i} be the instantaneous SINRs of OFDM subcarriers used to transmit $\hat{X}_{p_i}$ and $\hat{X}_{q_i}$, respectively. The *condition number* β_i is then defined as [13]

$$\beta_i \triangleq \sqrt{\frac{\gamma_{q_i}}{\gamma_{p_i}}}. \tag{12}$$

The optimal ${\theta_k}^{opt}$ are given in [13]

$${\theta_i}^{opt} = \begin{cases} \pi/4 & \beta_i \leq \sqrt{3} \\ \tan^{-1}\left\{ \begin{matrix} -\sqrt{({\beta_i}^2-1)^2-{\beta_i}^2} \\ +\ ({\beta_i}^2-1) \end{matrix} \right\} & \beta_i > \sqrt{3}. \end{cases} \tag{13}$$

and ${\theta_i}^{opt}$ are computed for $i = 1, ..., N_x/2$, and used to generate the corresponding coded symbol pairs at the transmitter. Then, $(\hat{X}_{p_i}, \hat{X}_{q_i})$ are mapped to N_x self-het OFDM subcarriers. If the channel state information available at the transmitter (CSIT), the selection of the optimum pair can be performed using the sorted instantaneous SINR vector [12] estimated at the transmitter. Otherwise, pairing must be performed with average SINR , i.e., subcarriers located far from the local RF carrier is paired with those located close to the local RF carrier.

At the receiver, the maximum likelihood decoding (MLD) is used to decode the original information symbols. Let $\hat{H}_{p_i}$, where $\hat{H}_{p_i} \triangleq H_c^* H_{N_g+i}$, and $\hat{H}_{q_i}$, where $\hat{H}_{q_i} \triangleq H_c^* H_{N-i+1}$, be the equivalent channel responses of the $(N_g + i)$-th and $(N - i + 1)$-th OFDM subcarriers, respectively. From (7), the received symbols of $(N_g + i)$-th and $(N - i + 1)$-th OFDM subcarriers can be written as

$$\begin{aligned} \hat{Y}_{p_i} &= A H_{p_i} \hat{X}_{p_i} + \hat{Z}_{p_i} \\ \hat{Y}_{q_i} &= A H_{q_i} \hat{X}_{q_i} + \hat{Z}_{q_i}. \end{aligned} \tag{14}$$

The MLD is performed to find the decoded information symbols in i-th pair as

$$\begin{aligned} \hat{a}_i &= \arg\min_{X \in \mathcal{X}} \left\{ \begin{matrix} |\Re\{H_{p_i}^* \hat{Y}_{p_i}\} - A|H_{p_i}|^2 \Re\{X \exp(j\theta_i)\}|^2 \\ +|\Re\{H_{q_i}^* \hat{Y}_{q_i}\} - A|H_{q_i}|^2 \Im\{X \exp(j\theta_i)\}|^2 \end{matrix} \right\} \\ \hat{b}_i &= \arg\min_{X \in \mathcal{X}} \left\{ \begin{matrix} |\Im\{H_{p_i}^* \hat{Y}_{p_i}\} - A|H_{p_i}|^2 \Re\{X \exp(j\theta_i)\}|^2 \\ +|\Im\{H_{q_i}^* \hat{Y}_{q_i}\} - A|H_{q_i}|^2 \Im\{X \exp(j\theta_i)\}|^2 \end{matrix} \right\} \end{aligned} \tag{15}$$

where $\mathcal{X}$ is the *M*-QAM constellation.

IV. Simulation Results

In this section, we present the simulation results of SCP and subcarrier pairing for self-het OFDM over the channel model introduced in Section II(A). SCP is conducted according to (9). The pairing scheme is based on (11) and the optimal rotation angles are chosen according to (13). In Table I, we provide a summary of key simulation parameters for our simulations. In Case (A), we consider a 60 GHz indoor radio environment, where the relevant parameters are taken from [9]. We note that the cluster and ray arrival rates are comparatively high, since it models an indoor environment. In Case (B), we consider a scenario where the cluster and ray arrival rates are moderate. This corresponds to a longer indoor space (e.g. open space office layouts).

TABLE I
Simulation parameters

Parameter	Case (A)	Case (B)
(Λ, λ)	(1/21.1 ns, 1/2.68 ns)	(1/40 ns, 1/15 ns)
(Γ, γ)	(22.3 ns, 17.2 ns)	(25 ns, 20 ns)
$(\sigma_1, \sigma_2, \sigma_\alpha)$	(7.27,4.42,3) dB	(7.27,4.42,3) dB
N	256	
T_s	2.5 ns	
η	0.6	
$(N_x,\ N_g)$	(128,128)	
Δf	1.5625 MHz	
P	10	
Modulation	4-QAM	

Fig. 3(a) compares the magnitude of channel response (i.e. $|H_k|$ in (4)) for the Cases (A) and (B), when there is no LOS signal (i.e. $\alpha = 0$). In case (A), we note that the channel response has a good agreement with the Rayleigh distribution due to the the higher cluster and ray arrival rates (see Fig. 3(b)). However, in Case (B), the channel is deviating from the Rayleigh distribution due to the low cluster and ray arrival rates, as shown in Fig. 3(c).

For NLoS channels, Fig. 4 shows the BER performance improvements by the proposed enhancements (i.e. SCP and subcarrier pairing technique) for both Case (A) and (B). In Case (A), the proposed enhancements offer combined SNR gain of 7.7 dB at BER of 10^{-2}, where SCP technique and subcarrier pairing scheme provide individual gains of 5 dB and 2.7 dB, respectively. We note that the improvements in Case (A) are approximately the same as the improvements obtained in a Rayleigh fading channel model. However, in Case (B), the BER performance are slightly better compared to Case (A), since the channel is not as severely faded as in Case (A) (see Fig. 3(a)). In Case (B), the proposed enhancements offer 7.2 dB combined gain at BER of 10^{-2}.

In Fig. 4, we also note the diversity order of standard self-het OFDM is less than 1, and the proposed enhancements help the self-het OFDM scheme to improve the diversity order significantly in both scenarios. This diversity improvement results from two factors: (*i*) the SCP technique significantly minimizes the outage problem experienced in standard self-het OFDM [11] and (*ii*) the IQ component interleaving and constellation rotation used in the subcarrier pairing scheme ensure that at least half the information associated with the original symbol pair (i.e. $\{(a_i, b_i), i = 1, ..., N_x/2\}$) is transmitted in the case of one channel suffers from deep fading [12].

Fig. 5 analyzes the variation of the SNR gains (i.e. from SCP and subcarrier pairing techniques) for channel Cases (A) and (B) with Rician *K*-factor. We note that the SNR gains

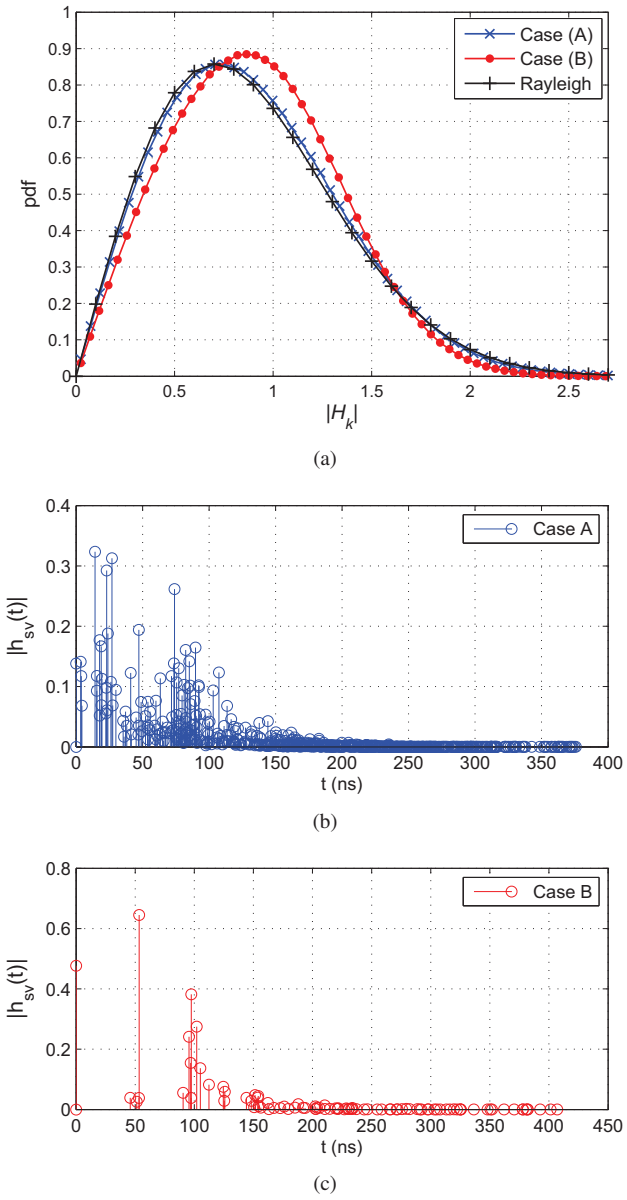

Fig. 3. (a) pdf of the channel response in Case (A) and Case (B) (b) An example channel impulse response (magnitude) of Case A (c) An example channel impulse response (magnitude) of Case B

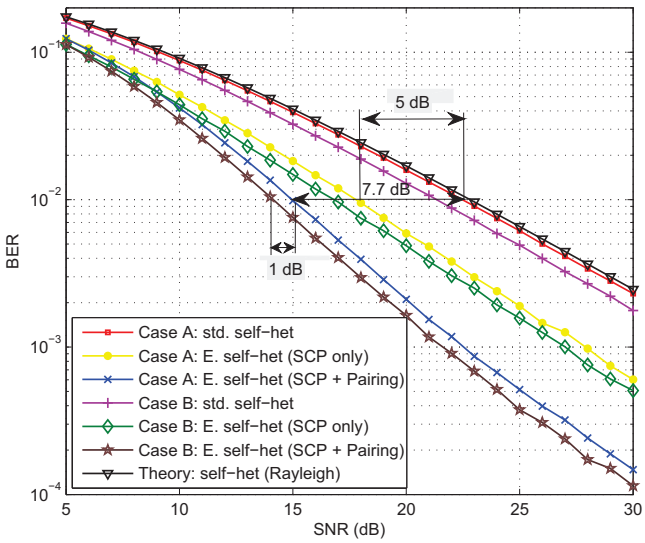

Fig. 4. BER performance of enhanced and standard self-het OFDM

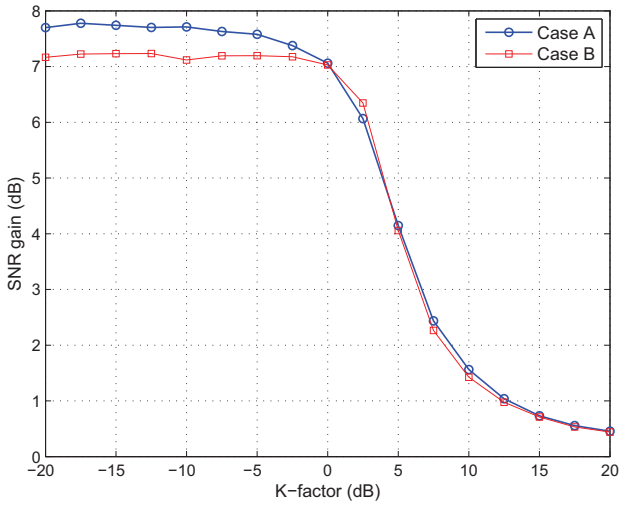

Fig. 5. Variation of SNR gain of proposed enhancements with Rician K-factor

for K-factor < -10B of channel Cases (A) and (B) are 7.7 dB and 7.2 dB, respectively. At $K = 0$, self-het OFDM enhancements contribute 7 dB SNR gain for both the channel cases. As shown in Fig. 5, those gains decrease with the K-factor. We note that proposed enhancements offer considerable improvements up to $K < 12.5$ dB, and then reach a fixed gain of 0.5 dB. This fixed 0.5 dB gain is due to the imbalance SNRs of OFDM subcarriers in LoS dominated channels [12].

V. Conclusion

This paper analyzes the enhanced self-het OFDM using SCP and subcarrier pairing over a practical 60 GHz indoor RF channel model. We show that, for channels with high ray and cluster arrival rates, the Rayleigh fading assumption is valid. Otherwise, the channel deviates significantly from standard Rayleigh fading models for NLoS. In such NLoS channels, the proposed enhancements improve diversity order and the BER performance of self-het OFDM by at least 7.7 dB at BER of 10^{-2}, when compared to the standard self-het OFDM. For LoS channels, the proposed enhancements improve the BER performance of self-het OFDM by 4 dB and 0.5 dB, given the channel Rician K-factor of 5 dB and 20 dB (i.e. a dominant LoS component appears), respectively. We finally note that SCP and subcarrier pairing require a relatively low complexity receiver structure and very limited feedback.

ACKNOWLEDGMENT

This work was performed within the Monash Software Defined Telecommunications Lab and supported by the Monash Professional Fellowship and ARC DP 130100336.

REFERENCES

[1] A. Armada, and M. Calvo, "Phase noise and subcarrier spacing effects on the performnace of an OFDM communication system," *IEEE Commun. Letters*, vol. 2, no. 1, pp. 11–13, Jan. 1998.

[2] Z. Lao, J. Jensen, K. Guinn, and M. Sokolich, "80-GHz differential VCO in InP SHBTs," *IEEE Microwave and Wireless Components Letters*, vol. 14, no. 9, pp. 407–409, Sept. 2004.

[3] C. Cao and K. O, "Millimeter-wave voltage-controlled oscillators in 0.13-μm CMOS technology," *IEEE Journal of Solid-State Circuits*, vol. 41, no. 6, pp. 1297–1304, June 2006.

[4] P. Smulders, "Exploiting the 60GHz band for local wireless multimedia access: prospects and future directions," *IEEE Comm. Magazine*, vol. 40, no. 1, pp. 140–147, Jan 2002.

[5] H.-J. Song and T. Nagatsuma, "Present and future of terahertz communications," *IEEE Trans. on Terahertz Science and Tech.*, vol. 1, no. 1, pp. 256–263, Sept. 2011.

[6] Y. Shoji, M. Nagatsuka, K. Hamaguchi, and H. Ogawa, "60GHz band 64 QAM/OFDM terrestrial digital broadcasting signal transmission by using millimeter-wave self-heterodyne system," *IEEE Trans. on Broadcasting*, vol. 47, no. 3, pp. 218–227, Sept. 2001.

[7] Y. Shoji, K. Hamaguchi, and H. Ogawa, "Millimeter-wave remote self-heterodyne system for extremely stable and low-cost broad-band signal transmission," *IEEE Trans. on Microwave Theory and Tech.*, vol. 50, no. 6, pp. 1458–1468, June 2002.

[8] S.K. Yong, P. Xia, A. Valdes-Garcia, "*60GHz Technology for Gbps WLAN and WPAN: From Theory to Practice*," 1st ed. John Wiley & Sons, Ltd, 2010.

[9] Y. Shoji, H. Sawada, C. Chang-Soon, and H. Ogawa, "A Modified SV-Model Suitable for Line-of-Sight Desktop Usage of Millimeter-Wave WPAN Systems," *IEEE Transactions on Antennas and Propagation*, vol. 54, no. 10, pp. 3664–3674, Oct. 2006.

[10] A.A.M.. Saleh, R. Valenzuela, "A Statistical Model for Indoor Multipath Propagation," *IEEE Journal on Selected Areas in Communications*, vol. 5, no. 2, pp. 128–137, Feb. 1987.

[11] N. Fernando, Y. Hong, and E. Viterbo, "Self-heterodyne OFDM transmission for frequency selective channels," *submitted to IEEE Trans. on Commun.*, 2012.

[12] N. Fernando, Y. Hong, and E. Viterbo, "Subcarrier Pairing for Self-Heterodyne OFDM," *submitted to IEEE ICC conf.*, 2012.

[13] S. Mohammed, E. Viterbo, Y. Hong, and A. Chockalingam, "MIMO precoding with X- and Y-codes," *IEEE Trans. on Inf. Theory*, vol. 57, no. 6, pp. 3542–3566, June 2011.

[14] J. Boutros and E. Viterbo, "Signal space diversity: a power- and bandwidth-efficient diversity technique for the Rayleigh fading channel," *IEEE Trans. on Inf. Theory*, vol. 44, no. 4, pp. 1453–1467, July 1998.

[15] S. Mohammed, E. Viterbo, Y. Hong, and A. Chockalingam, "Precoding by pairing subchannels to increase MIMO capacity with discrete input alphabets," *IEEE Trans. on Inf. Theory*, vol. 57, no. 7, pp. 4156–4169, July 2011.

[16] Y. Hong, A. J. Lowery, and E. Viterbo, "Sensitivity improvement and carrier power reduction in direct-detection optical OFDM systems by subcarrier pairing," *Opt. Express*, vol. 20, no. 2, pp. 1635–1648, Jan. 2012.

[17] Y. Hong, E. Viterbo, and A. J. Lowery, "Improving the sensitivity of Direct-Detection optical OFDM systems by pairing of the optical subcarriers," in *37th European Conference and Exposition on Optical Communications*, Optical Society of America, 2011, pp. Th.11.B.2.

[18] S. Wu and Y. Bar-Ness, "OFDM systems in the presence of phase noise: consequences and solutions," *IEEE Trans. on Commun.*, vol. 52, no. 11, pp. 1988–1996, Nov. 2004.